INTERNATIONAL JOURNAL FOR NUMERICAL METHODS IN FLUIDS
Int. J. Numer. Meth. Fluids 2010; **64**:443–472
Published online 23 September 2009 in Wiley Online Library (wileyonlinelibrary.com). DOI: 10.1002/fld.2164

Adjoint-based design of shock mitigation devices

Arthur Stück[1,*,†], Fernando F. Camelli[2] and Rainald Löhner[2]

[1]*Institute for Fluid Dynamics and Ship Theory, Hamburg University of Technology, Schwarzenbergstraße 95 C, D-21073 Hamburg, Germany*
[2]*CFD Center, Department of Computational and Data Science, M.S. 6A2, College of Science, George Mason University, Fairfax, VA 22030-4444, U.S.A.*

SUMMARY

Unsteady Euler and adjoint Euler solvers have been combined in order to aid in the design of shock mitigation devices. The flowfield is integrated forward in time and stored. The adjoint is then integrated going backwards in time, restoring and interpolating the saved Euler solution to the current point in time. The gradient is obtained from a surface integral formulation during the adjoint run. Comparisons of adjoint-based and finite-differencing gradients for different verification cases show less than 10% deviation. The results obtained indicate that this is a very cost-effective way to obtain the gradients of an objective function with respect to surface design changes. Moreover, as the sensitivity information is determined over a complete surface, the procedure provides considerable insight, and can efficiently facilitate the design of shock mitigation devices such as architecturally appealing blast walls. Copyright © 2009 John Wiley & Sons, Ltd.

Received 26 December 2008; Revised 21 May 2009; Accepted 18 July 2009

KEY WORDS: shock mitigation; Euler solvers; adjoint-based design; unsteady adjoints; finite elements; CFD

1. INTRODUCTION

Explosions remain the most frequently used form of terror attack. They represent a low-tech, cheap, abundantly available resource that produces the desired destructive, psychological (mainly fear and rage), publicity (monopolization of news), economical (disruption of travel, commerce, investment and consumption) and political (destabilization) effects. Most buildings are designed and built to the usual civil engineering criteria: gravity, water, wind, snow, earthquakes, occupancy and vibration loads. This implies that no consideration is taken for potential blast loads, making most of them vulnerable to attacks. Traditional ways to mitigate blast effects include the establishment of safe distance perimeters, reinforcement of windows and walls, as well as walls and other protective structures.

*Correspondence to: Arthur Stück, Institute for Fluid Dynamics and Ship Theory, Hamburg University of Technology, Schwarzenbergstraße 95 C, D-21073 Hamburg, Germany.
†E-mail: arthur.stueck@tu-harburg.de

Many consulates, embassies and military bases are located in city environments. This makes it almost impossible to place 'safe areas' around them, and to obtain allowances for edification of (mostly 'high and ugly') blast walls. In order to obtain the desired effect of shielding while satisfying the aesthetic outlay required by urban environments, these walls have to be designed optimally.

Assuming that the amount and the location of the explosive, the location of critical damage areas (windows, facilities) and the design constraints for protective structures are given, one can recast the design of the protective structure or shock mitigation device (e.g. a blast wall) as an optimal shape design problem [1–7]: Change the protective structure in such a way as to satisfy the design constraints and minimize the effects of a blast. The input parameters for this optimal shape design problem define the form of the protective structure (e.g. a series of splines defining a wall). The output parameter is the damage done by the blast for a given shape of the protective structure, and is typically measured in terms of peak pressure and impulse.

Optimization techniques commonly employed include genetic algorithms [7–11], as well as gradient-based methods [1–5, 7, 12, 13]. Given N design parameters, genetic algorithms require $O(N^2)$ function evaluations (i.e. unsteady 3-D computational fluid dynamics (CFD) runs) for convergence. Gradient-based techniques typically require a fixed number of steps to converge, but in each of these steps the gradient vector of the cost function with respect to the shape parameters must be computed. If the gradients are evaluated via finite differences (FD), this implies $O(N)$ cost-function evaluations. If, on the other hand, adjoint solvers are employed, the gradients may be obtained at the numerical effort of $O(1)$ cost-function evaluation(s). Given the high cost of a typical unsteady 3-D CFD run, using genetic algorithms or FD gradient-based techniques for optimization becomes onerous, and leaves adjoint-based techniques as the obvious choice. In this way, the adjoint approach allows for in-depth sensitivity studies in practical design problems which would be prohibitive otherwise. The number of design parameters does not need to be cut down *a priori* by guessing, or according to the designer's experience. As presented in the following, it can be visualized to give a detailed insight into the problem from a target point of view.

The remainder of the paper is organized as follows: Sections 2–4 treat the description of the Euler flow problem, the adjoint problem, the evaluation of gradients and the cost functions considered. The attention then turns to the flow and adjoint solvers employed, as well as implementational issues for transient adjoint problems (Sections 5–7). This is followed by verification studies and examples for the adjoint sensitivity analysis (Sections 8 and 9). Some thoughts on further prospects and opportunities the proposed calculus offers, as well as conclusions and outlook complete the exposition (Sections 10 and 11). In order to keep the paper concise and easily readable, parts of the derivations have been confined to the Appendix. Throughout the following Einstein's notation applies to the lower-case Latin subscripts, unless bracketed or declared exceptionally. When symbolic notation is used the number of underlines corresponds to the order of the tensor; if present, the differentiation index is the first tensor index.

2. EULER-BASED EVALUATION OF SHOCK EFFECTS

Given the situation sketched in Figure 1, let us define a cost function J representing the damage to a building due to a blast. For a given explosive amount and blast location(s), this function will depend on the geometry of the setup (location, height and form of the protective walls and

DOI: 10.1002/fld

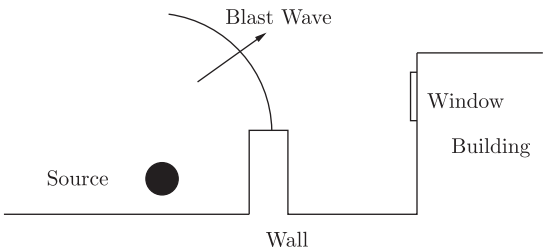

Figure 1. Protective wall in front of a building.

buildings, etc.), which is described by a series of parameters $\underline{\beta}$. These in turn influence the resulting blast flowfield $\underline{U}(\underline{\beta})$ and the damage J, viz.

$$J(\underline{\beta}, \underline{U}(\underline{\beta})) \tag{1}$$

The flow domain is represented by Ω, its boundary is denoted by Γ. The damage criteria or cost functions are defined on sensitive parts of the building being attacked (such as windows, doorways, etc.), referred to as *target surfaces* $\Gamma_{\text{trg}} \subset \Gamma$. The boundary parts subject to the shape parameterization $\underline{\beta}$ are so-called *design surfaces* $\Gamma_{\text{dsg}} \subset \Gamma$ representing blast walls, protective structures or other blast mitigation devices. Assuming the common case that design surfaces and target surfaces have no intersection, $\Gamma_{\text{trg}} \cap \Gamma_{\text{dsg}} = \emptyset$, leads to

$$J(\underline{U}(\underline{\beta})) \tag{2}$$

Thus, the design only affects the cost function via the flowfield. The following analysis is presented for the general case (1) first, and subsequently confined to (2).

Consider a generic cost function containing volume and boundary contributions:

$$J = J_\Omega + J_\Gamma = \int_0^T \int_{\Omega_{\text{trg}}} j_\Omega \, \mathrm{d}\Omega \, \mathrm{d}t + \int_0^T \int_{\Gamma_{\text{trg}}} j_\Gamma \, \mathrm{d}\Gamma \, \mathrm{d}t \tag{3}$$

The spatial integration is carried out over the target surface Γ_{trg} or volume Ω_{trg} respectively. The optimization is subject to the physics of the problem, which for the class of problems treated here is well described by the unsteady Euler equations

$$\underline{R} = \frac{\partial \underline{U}}{\partial t} + \frac{\partial \underline{F}_i}{\partial x_i} = \frac{\partial \underline{U}}{\partial t} + \frac{\partial \underline{U}}{\partial x_i} \cdot \frac{\partial \underline{F}_i}{\partial \underline{U}} = \frac{\partial \underline{U}}{\partial t} + \underline{\underline{A}}_i \cdot \frac{\partial \underline{U}}{\partial x_i} = 0 \tag{4}$$

with the vector of the conservative variables $\underline{U}$ and the fluxes $\underline{F}_j$

$$\underline{U} = \begin{pmatrix} \rho \\ \rho v_i \\ \rho e \end{pmatrix}, \quad \underline{F}_j = \begin{pmatrix} \rho v_j \\ \rho v_j v_i + p\delta_{ij} \\ v_j (\rho e + p) \end{pmatrix} \tag{5}$$

where ρ, v_i and e denote the fluid density, the Cartesian velocity components and the total energy, and $\underline{\underline{A}}_i$ are the Jacobian matrices. The pressure p is linked to the primitive flow variables (ρ, v_i, e) through the polytropic gas equation

$$p = (\gamma - 1)\rho(e - v_k v_k/2) \tag{6}$$

DOI: 10.1002/fld

with the ratio of the specific heats γ. The boundary conditions are as follows:

- For *walls* the normal velocity vanishes ($n_j v_j = 0$).
- For *lines* where re-entrant surfaces meet the velocity is tangential to the line ($\underline{v} = |\underline{v}|\underline{t}$).
- For *far-field boundaries* vanishing gradients of the unknowns or characteristic boundary conditions are imposed [7].

3. UNSTEADY ADJOINT FORMULATION

A shape variation $\delta\underline{\beta}$ will lead to displacements $\delta\underline{x}(\delta\underline{\beta})$ of both boundary and interior nodes of the computational mesh. The linear variation of the flow variables with respect to a nodal shift $\delta\underline{x}$ is given by

$$\delta\underline{U}^{(lc)} = \delta\underline{U}^{(l)} + \delta\underline{U}^{(c)} = \delta\underline{U}^{(l)} + \delta\underline{x} \cdot \nabla\underline{U} \tag{7}$$

It contains the *local* variation $\delta\underline{U}^{(l)}$ (flow variation at the 'old' position) and the *convective* variation $\delta\underline{U}^{(c)}$ (flow variation due to a position shift $\delta\underline{x}$ obtained from a truncated Taylor series expansion of the 'old' Euler flow). Accordingly, the *total* variation of a cost function is written as

$$\delta J^{(t)} = \delta J^{(lc)} + \delta J^{(g)} = \delta J^{(l)} + \delta J^{(c)} + \delta J^{(g)} \tag{8}$$

wherein $\delta J^{(g)}$ denotes the *geometric* variation due to changes of the domain volume $\delta\Omega$ and its boundary $\delta\Gamma$. The convective and geometric variations can easily be computed after adapting the computational mesh to the shape variation. Evaluating the local variations would require the solution of the linearized flow problem for $\delta\underline{U}^{(l)}$ for each shape parameter. As one linearized flow solution requires roughly the same numerical effort as a nonlinear reference solution the numerical costs quickly become prohibitive. Alternatively, the local variations can be eliminated by solving the adjoint problem instead, so that the numerical effort for evaluating the gradients practically becomes independent of the number of shape parameters.

3.1. Extended cost function

The optimization problem subject to the Euler constraints can be transformed into an unconstrained problem via the Lagrange method. The extended cost function (also knowns as the Lagrange polynomial) reads:

$$L = J + \int\int \underline{\hat{U}} \cdot \underline{R}\, \mathrm{d}\Omega\, \mathrm{d}t \tag{9}$$

where $\underline{\hat{U}} = (\hat{\rho}, \hat{v}_j, \hat{e})$ are the Lagrange multipliers or adjoint variables. The spatial integration is carried out over the whole domain Ω or its boundary Γ, unless otherwise identified. Note that the base units of the adjoint multipliers depend on the definition of both cost function and constraints. The cost function change with a shape variation can be expressed as the total variation of the Lagrange polynomial:

$$\delta J^{(t)} = \delta L^{(t)} = \int_0^T \int \underline{\hat{U}} \cdot \underline{R}\, \mathrm{d}(\delta\Omega)\, \mathrm{d}t \tag{10a}$$

$$+ \int_0^T \int \delta\underline{\hat{U}}^{(lc)} \cdot \underline{R}\, \mathrm{d}\Omega\, \mathrm{d}t \tag{10b}$$

DOI: 10.1002/fld

$$+\int_0^T \int \underline{\hat{U}} \cdot \delta \underline{R}^{(lc)} \, \mathrm{d}\Omega \, \mathrm{d}t \tag{10c}$$

$$+\int_0^T \left[\int_{\Omega_{\mathrm{trg}}} j_\Omega^{(lc)} \, \mathrm{d}\Omega + \int_{\Gamma_{\mathrm{trg}}} j_\Gamma^{(lc)} \, \mathrm{d}\Gamma \right] \mathrm{d}t \tag{10d}$$

$$+\int_0^T \left[\int_{\Omega_{\mathrm{trg}}} j_\Omega \, \mathrm{d}(\delta\Omega) + \int_{\Gamma_{\mathrm{trg}}} j_\Gamma \, \mathrm{d}(\delta\Gamma) \right] \mathrm{d}t \tag{10e}$$

As the Euler constraints, Equation (4), are satisfied at the current state, both the geometric variation of the cost function extension (10a) and the contributions from the local/convective variations of the Lagrange multipliers (10b) are zero. Equation (4) implies that also the respective gradients of the Euler residuals vanish identically and the convective variation of the Euler equations in (10c) is zero: $\delta \underline{R}^{(c)} = \delta \underline{x} \cdot \nabla \underline{R} = 0$. The remaining terms comprise the local variations of the Euler equations (10c), the local/convective variations of the cost function (10d) and the geometric variation of the cost function (10e). Equation (10) can be rewritten as

$$\delta J^{(t)} = \int_0^T \int \left[\frac{\partial \delta \underline{U}^{(l)}}{\partial t} + \frac{\partial}{\partial x_i} \left(\delta \underline{U}^{(l)} \cdot \frac{\partial \underline{F}_i}{\partial \underline{U}} \right) \right] \cdot \underline{\hat{U}} \, \mathrm{d}\Omega \, \mathrm{d}t \tag{11a}$$

$$+\int_0^T \left[\int_{\Omega_{\mathrm{trg}}} \delta \underline{U}^{(lc)} \cdot \frac{\partial j_\Omega}{\partial \underline{U}} \, \mathrm{d}\Omega + \int_{\Gamma_{\mathrm{trg}}} \delta \underline{U}^{(lc)} \cdot \frac{\partial j_\Gamma}{\partial \underline{U}} \, \mathrm{d}\Gamma \right] \mathrm{d}t \tag{11b}$$

$$+\int_0^T \left[\int_{\Omega_{\mathrm{trg}}} j_\Omega \, \mathrm{d}(\delta\Omega) + \int_{\Gamma_{\mathrm{trg}}} j_\Gamma \, \mathrm{d}(\delta\Gamma) \right] \mathrm{d}t \tag{11c}$$

Using integration by parts with respect to time and space, Equation (11) can be rearranged to read

$$\delta J^{(t)} = \int_0^T \left[\int \delta \underline{U}^{(l)} \cdot \left(-\frac{\partial \underline{\hat{U}}}{\partial t} - \frac{\partial \underline{F}_i}{\partial \underline{U}} \cdot \frac{\partial \underline{\hat{U}}}{\partial x_i} \right) \mathrm{d}\Omega + \int_{\Omega_{\mathrm{trg}}} \delta \underline{U}^{(lc)} \cdot \frac{\partial j_\Omega}{\partial \underline{U}} \, \mathrm{d}\Omega \right] \mathrm{d}t \tag{12a}$$

$$+\int_0^T \left[\int \delta \underline{U}^{(l)} \cdot \frac{\partial \underline{F}_i}{\partial \underline{U}} \cdot \underline{\hat{U}} \, n_i \, \mathrm{d}\Gamma + \int_{\Gamma_{\mathrm{trg}}} \delta \underline{U}^{(lc)} \cdot \frac{\partial j_\Gamma}{\partial \underline{U}} \, \mathrm{d}\Gamma \right] \mathrm{d}t \tag{12b}$$

$$+\left[\int \delta \underline{U}^{(l)} \cdot \underline{\hat{U}} \, \mathrm{d}\Omega \right]_0^{\mathrm{T}} \tag{12c}$$

$$+\int_0^T \left[\int_{\Omega_{\mathrm{trg}}} j_\Omega \, \mathrm{d}(\delta\Omega) + \int_{\Gamma_{\mathrm{trg}}} j_\Gamma \, \mathrm{d}(\delta\Gamma) \right] \mathrm{d}t \tag{12d}$$

with n_i representing the boundary unit vector.

DOI: 10.1002/fld

3.2. Adjoint Euler equations

The adjoint Euler problem—consisting of the adjoint field equations, boundary and initial conditions—is solved in order to eliminate all local variations within Equation (12). The adjoint field equations are obtained from the right-hand side terms of (12a):

$$\begin{aligned} -\frac{\partial \underline{\hat{U}}}{\partial t} - \frac{\partial \underline{F}_i}{\partial \underline{U}} \cdot \frac{\partial \underline{\hat{U}}}{\partial x_i} = -\frac{\partial \underline{\hat{U}}}{\partial t} - \underline{\underline{A}}_i^{\mathrm{T}} \cdot \frac{\partial \underline{\hat{U}}}{\partial x_i} = 0 \quad \text{in } \Omega \backslash \Omega_{\mathrm{trg}} \\ -\frac{\partial \underline{\hat{U}}}{\partial t} - \underline{\underline{A}}_i^{\mathrm{T}} \cdot \frac{\partial \underline{\hat{U}}}{\partial x_i} + \frac{\partial j_\Omega}{\partial \underline{U}} = 0 \quad \text{in } \Omega_{\mathrm{trg}} \end{aligned} \tag{13}$$

Note that:

- A *linear* system of *advection equations* is obtained.
- The eigenvalues of this system are the same as those of the original PDE.
- Owing to the negative sign in front of the Jacobians $\underline{\underline{A}}_i$, the 'advection direction' for the adjoint is opposite to the advection direction of the original PDE ($\underline{R}$).
- The temporal integration goes backwards, that is, in the opposite direction of usual time; thus, when solving for the adjoint, one starts at the end of the flow run and moves back until reaching the start time.
- As the flow variables $\underline{U}$ vary in time, so do the Jacobians $\underline{\underline{A}}_i$; this implies that an expeditious way to (re-)store this information in time has to be found.

The adjoint boundary conditions have to be chosen such that the local variations in (12b) on the non-perturbed boundary are eliminated:

$$\begin{aligned} \delta \underline{U}^{(l)} \cdot \frac{\partial \underline{F}_n}{\partial \underline{U}} \cdot \underline{\hat{U}} = 0 \quad \text{on } \Gamma \backslash \Gamma_{\mathrm{trg}} \\ \delta \underline{U}^{(l)} \cdot \left[\frac{\partial \underline{F}_n}{\partial \underline{U}} \cdot \underline{\hat{U}} + \frac{\partial j_\Gamma}{\partial \underline{U}} \right] = 0 \quad \text{on } \Gamma_{\mathrm{trg}} \end{aligned} \tag{14}$$

A detailed analysis of the adjoint boundary conditions is given in Appendix A.1. The controlled boundaries are considered in Section 4 in order to obtain the cost function gradient. Equations (13) and (14) indicate that the adjoint field equations and boundary conditions are cost function specific. A detailed analysis of the adjoint boundary conditions is given in the Appendix. The choice

$$\underline{\hat{U}}(t = T) = 0 \quad \text{in } \Omega \tag{15}$$

eliminates the local variations in (12c) at $t = T$. As the adjoint solver runs in reverse time this is referred to as adjoint 'initialization'.

The blast flow initialization is assumed to be independent of the shape of the protective structure (design surface), that is,

$$\delta \underline{U}^{(l)}(t = 0) = 0 \quad \text{in } \Omega \tag{16}$$

which eliminates the remaining contributions to (12c). The terms in (12d) are irrelevant to the adjoint problem as they do not contain local variations.

DOI: 10.1002/fld

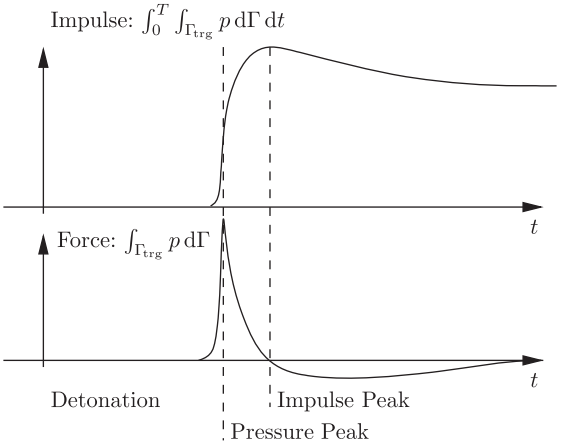

Figure 2. Target force and impulse due to blast effects.

3.3. Cost functions considered

The cost functions considered for the evaluation of blast mitigation devices are only declared on the boundaries of the flow domain, hence $J_\Omega = 0$. However, taking into account volume-based cost functions as indicated in the analysis above is straightforward. We are confining ourselves to cases where the target surface(s) are not subject to shape variations, that is $\Gamma_{\text{trg}} \cap \Gamma_{\text{dsg}} = \emptyset$. Therefore, both the convective variations in the second term of (12b) and the geometric contributions (12d) are zero, $\delta J_\Gamma^{(c)} = \delta J_\Gamma^{(g)} = 0$.

Blast effects may be analyzed in terms of the pressures, forces or impulses the target is exposed to. Figure 2 shows possible force and impulse loads caused by a detonation. The cost functions listed below have been considered for the quantification of blast effects.

(i) The impulse I on a target area (such as a window) caused by pressure values greater than ambient pressure p_0:

$$J_{\Gamma 1} = I = \int_0^T \int_{\Gamma_{\text{trg}}} j_{\Gamma 1}\,\mathrm{d}\Gamma\,\mathrm{d}t = \int_0^T \int_{\Gamma_{\text{trg}}} \max(p - p_0, 0)\,\mathrm{d}\Gamma\,\mathrm{d}t \tag{17}$$

$$\delta J_{\Gamma 1}^{(l)} = \delta I^{(l)} = \int_0^T \int_{\Gamma_{\text{trg}}} \delta p^{(l)} \frac{\partial j_{\Gamma 1}}{\partial p}\,\mathrm{d}\Gamma\,\mathrm{d}t \tag{18}$$

with

$$\frac{\partial j_{\Gamma 1}}{\partial p} = \frac{\max(p - p_0, 0)}{p - p_0 + \varepsilon}$$

A small value ε is added to the denominator to avoid singularities.

DOI: 10.1002/fld

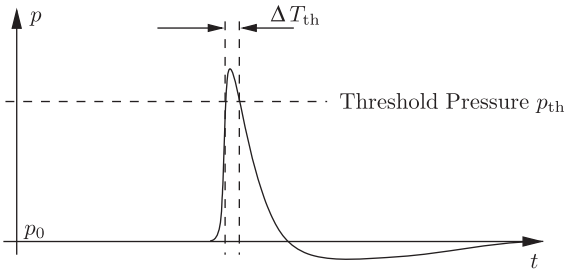

Figure 3. Pressure peak: pressure over time.

(ii) The mean pressure peaks $\overline{p}$ acting upon the target face:

$$J_{\Gamma 2} = \overline{p} = \int_0^T \int_{\Gamma_{\text{trg}}} j_{\Gamma 2} \, \mathrm{d}\Gamma \, \mathrm{d}t$$

$$= \frac{1}{A_{\text{trg}} \Delta T_{\text{th}}} \int_0^T \int_{\Gamma_{\text{trg}}} \frac{\max(p - p_{\text{th}}, 0)}{p - p_{\text{th}} + \varepsilon} (p - p_0) \, \mathrm{d}\Gamma \, \mathrm{d}t \tag{19}$$

$$\delta J_{\Gamma 2}^{(l)} = \delta \overline{p}^{(l)} = \int_0^T \int_{\Gamma_{\text{trg}}} \delta p^{(l)} \frac{\partial j_{\Gamma 2}}{\partial p} \, \mathrm{d}\Gamma \, \mathrm{d}t \tag{20}$$

with

$$\frac{\partial j_{\Gamma 2}}{\partial p} = \frac{1}{A_{\text{trg}} \Delta T_{\text{th}}} \frac{\max(p - p_{\text{th}}, 0)}{p - p_{\text{th}} + \varepsilon}$$

ΔT_{th} denotes the period of time while the pressure threshold p_{th} is exceeded anywhere on the target window area A_{trg} as shown in Figure 3. A variation of ΔT_{th} has not been taken into consideration.

(iii) The quadratic positive deviation from a threshold pressure value p_{th}:

$$J_{\Gamma 3} = \int_0^T \int_{\Gamma_{\text{trg}}} j_{\Gamma 3} \, \mathrm{d}\Gamma \, \mathrm{d}t$$

$$= \int_0^T \int_{\Gamma_{\text{trg}}} \frac{1}{2} [\max(p - p_{\text{th}}, 0)]^2 \, \mathrm{d}\Gamma \, \mathrm{d}t \tag{21}$$

$$\delta J_{\Gamma 3}^{(l)} = \int_0^T \int_{\Gamma_{\text{trg}}} \delta p^{(l)} \frac{\partial j_{\Gamma 3}}{\partial p} \, \mathrm{d}\Gamma \, \mathrm{d}t \tag{22}$$

with

$$\frac{\partial j_{\Gamma 3}}{\partial p} = \max(p - p_{\text{th}}, 0)$$

DOI: 10.1002/fld

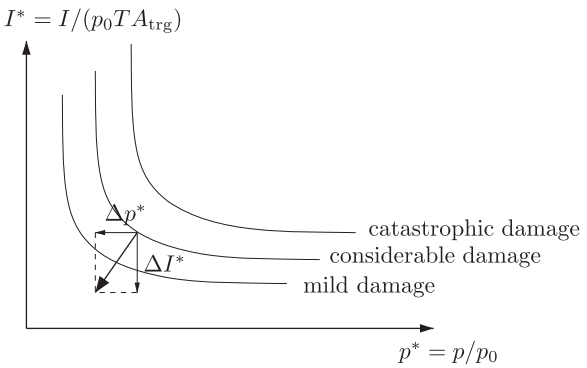

Figure 4. Optimal cost function ratio $\Delta p^*/\Delta I^*$ for a damage reduction according to the pressure–impulse diagram.

(iv) A case-specific weighting of $\delta J_{\Gamma 1}^{(l)}$ and $\delta J_{\Gamma 2}^{(l)}$ according to the pressure–impulse diagram (Figure 4):

$$\begin{aligned}\delta J_{\Gamma 4}^{(l)} &= \alpha \delta J_{\Gamma 1}^{*(l)} + (1-\alpha)\delta J_{\Gamma 2}^{*(l)} \\ &= \alpha \frac{\delta J_{\Gamma 1}^{(l)}}{A_{\mathrm{trg}} T p_0} + (1-\alpha)\frac{\delta J_{\Gamma 2}^{(l)}}{p_0}\end{aligned} \tag{23}$$

with

$$\alpha = \left(\frac{\Delta p^*}{\Delta I^*} + 1\right)^{-1}$$

Δp^* and ΔI^* are defined in Figure 4, using the asterisk notation for nondimensional values. Thus,

$$\delta J_{\Gamma 4}^{*(l)} = \int_0^T \int_{\Gamma_{\mathrm{trg}}} \delta p^{(l)} \frac{\partial j_{\Gamma 4}}{\partial p} \,\mathrm{d}\Gamma \,\mathrm{d}t \tag{24}$$

with

$$\frac{\partial j_{\Gamma 4}}{\partial p} = \frac{1}{A_{\mathrm{trg}} p_0}\left[\frac{\alpha}{T}\frac{\max(p-p_0,0)}{p-p_0+\varepsilon} + \frac{1-\alpha}{\Delta T_{\mathrm{th}}}\frac{\max(p-p_{\mathrm{th}},0)}{p-p_{\mathrm{th}}+\varepsilon}\right]$$

A detailed derivation of the adjoint boundary conditions is given in the Appendix A.1. Depending on the cost function choice the boundary conditions are

$$\begin{aligned}&\underline{\hat{v}}\cdot\underline{n} = -\frac{\partial j_\Gamma}{\partial p}(\underline{x},t) \quad \text{for wall boundaries on } \Gamma_{\mathrm{trg}} \\ &\underline{\hat{v}}\cdot\underline{n} = 0 \quad \text{for wall boundaries on } \Gamma\backslash\Gamma_{\mathrm{trg}}\end{aligned} \tag{25}$$

For both Euler and adjoint Euler flow, only the normal velocity component is prescribed along the wall boundaries.

DOI: 10.1002/fld

4. GRADIENT EQUATION

The gradients of the negative objective functions ($J_{\Gamma 1\text{-}4}$) with respect to normal perturbations $\delta n = \underline{n} \cdot \delta \underline{x}$ indicate in which way the shape should be modified to achieve the desired effect. This information, when displayed graphically, gives the analyst or designer a clear insight into the design problem at hand.

Having eliminated the local variations in (12b) on the nonperturbed boundary by satisfying the adjoint boundary conditions, the remaining terms on the controlled boundary Γ_{dsg} define the cost function variation:

$$\delta J^{(t)} = \int_0^T \int_{\Gamma_{\text{dsg}}} \delta \underline{U}^{(l)} \cdot \frac{\partial \underline{F}_i}{\partial \underline{U}} \cdot \underline{\hat{U}} n_i \, \mathrm{d}\Gamma \, \mathrm{d}t \tag{26}$$

Demanding that the perturbed flow v_n^{new} satisfies the no-flux boundary condition ($v_j n_j|_{\text{wall}} = 0$) at the modified boundary location $\underline{x}_{\text{new}}$ leads to

$$0 = v_n^{\text{old}}|_{\underline{x}_{\text{old}}} = v_n^{\text{new}}|_{\underline{x}_{\text{new}}} \approx [v_n^{\text{old}} + \delta v_n^{(l)} + \delta v_n^{(c)}]_{\underline{x}_{\text{old}}} \rightsquigarrow \delta v_n^{(l)} = -\delta n \frac{\partial v_n}{\partial n} \text{ on old } \Gamma_{\text{dsg}} \tag{27}$$

Confined to boundary-normal perturbations δn and $\Gamma_{\text{trg}} \cap \Gamma_{\text{dsg}} = \emptyset$, the gradient equation reduces to (see Appendix A.2., Equations (A4) and (A5)):

$$\frac{\delta J^{(t)}}{\delta n} = \int_0^T \int_{\Gamma_{\text{dsg}}} -\frac{\partial v_n}{\partial n} [\rho \hat{\rho} + \rho v_i \hat{v}_i + (\rho e + p)\hat{e}] \, \mathrm{d}\Gamma \, \mathrm{d}t \tag{28}$$

This simple surface integral is referred to as adjoint post-processing. Volume grid deformation is not necessary and the gradient can be evaluated on the design surface alone. It is visualized by plotting the local cost function change per volume change δV over the design surface:

$$\frac{\delta J^{(t)}}{\delta V} = \int_0^T -\frac{\partial v_n}{\partial n} [\rho \hat{\rho} + \rho v_i \hat{v}_i + (\rho e + p)\hat{e}] \, \mathrm{d}t \quad \text{on } \Gamma_{\text{dsg}} \tag{29}$$

As the boundary vector is directed outwards, a positive volume change δV corresponds to an increased flow domain volume (or a reduced solid volume). Knowing the sensitivity distribution on the design surface allows for goal-oriented changes in the setup to achieve an increased blast resistance at minimum costs. Depending on the user's optimization strategy, the sensitivities can be applied to guide either manual or automatic optimization procedures.

5. FLOW SOLVER

Any finite volume or finite element discretization of Equation (4) will yield a discrete system of the form:

$$\underline{\underline{M}} \cdot \frac{\partial \underline{U}}{\partial t} = \underline{r}(\underline{U}) \tag{30}$$

or in index notation:

$$M_{ij} \frac{\partial U_j}{\partial t} = C_{ij} \mathscr{F}_j^{(ij)} = r_i \tag{31}$$

DOI: 10.1002/fld

Here, $M_{ij}, U_j, C_{ij}, \mathscr{F}_j^{(ij)}$ denote the mass-matrix, vector of unknowns, edge-coefficients for fluxes and edge-fluxes, respectively. This system is integrated in time using an explicit k-step minimal-storage Runge-Kutta scheme of the form:

$$\underline{\underline{M}} \cdot (\underline{U}^{(n+i/k)} - \underline{U}^{(n)}) = \alpha^{(i)} \Delta t \underline{r}(\underline{U}^{(n+(i-1)/k)}), \quad \alpha^{(i)} = \frac{1}{k-i+1} \tag{32}$$

The standard Galerkin approximation results in

$$\underline{\mathscr{F}}^{(ij)} = \underline{f}^{(i)} + \underline{f}^{(j)} \tag{33}$$

i.e. an equal weighting of the fluxes $\underline{f}^{(i)}, \underline{f}^{(j)}$ at the end-points i, j of an edge. This (high-order) combination of fluxes, which is known to lead to an unstable discretization, is augmented by stabilizing terms to achieve a stable scheme. Of the many possible options (see [7]) we include the widely used Roe solver [14], given by

$$\underline{\mathscr{F}}^{(ij)} = \underline{f}^{(i)} + \underline{f}^{(j)} - |\underline{\underline{A}}^{(ij)}| \cdot (\underline{U}^{(i)} - \underline{U}^{(j)}) \tag{34}$$

where $|\underline{\underline{A}}^{(ij)}|$ denotes the standard Roe matrix evaluated in the direction $\underline{l}^{(ji)} = \underline{x}^{(j)} - \underline{x}^{(i)}$, and $\underline{x}^{(i)}, \underline{x}^{(j)}$ are the coordinates of the end-points i, j of the edge. The dissipation is reduced by diminishing in a controlled manner the difference $\underline{U}^{(i)} - \underline{U}^{(j)}$ via reconstruction and limiting techniques. The results shown here were obtained with the van Albada limiter on conserved variables.

6. ADJOINT SOLVER

The adjoint Euler equations

$$\begin{aligned} -\frac{\partial \hat{\underline{U}}}{\partial t} - \underline{\underline{A}}_i^{\mathrm{T}} \cdot \frac{\partial \hat{\underline{U}}}{\partial x_i} &= 0 \quad \text{in } \Omega \backslash \Omega_{\mathrm{trg}} \\ -\frac{\partial \hat{\underline{U}}}{\partial t} - \underline{\underline{A}}_i^{\mathrm{T}} \cdot \frac{\partial \hat{\underline{U}}}{\partial x_i} &= -\frac{\partial j_\Omega}{\partial \underline{U}} \quad \text{in } \Omega_{\mathrm{trg}} \end{aligned} \tag{35}$$

may be discretized in the same way as the Euler equations, resulting in a system similar to that given by Equation (30). As the system is linear, a simpler numerical scheme may be employed. The consistent numerical fluxes used here are given by

$$\hat{\underline{\mathscr{F}}}^{(ij)} = \hat{\underline{f}}^{(i)} + \hat{\underline{f}}^{(j)} - |\lambda^{(ij)}| \left[\hat{\underline{U}}^{(i)} - \hat{\underline{U}}^{(j)} + \frac{\beta}{2} \underline{l}^{(ji)} \cdot (\nabla \hat{\underline{U}}^{(i)} + \nabla \hat{\underline{U}}^{(j)}) \right] \tag{36}$$

where $\lambda = |\underline{v}| + c$, $c = \sqrt{\gamma p/\rho}$ is the maximum eigenvalue of the system and $0 < \beta < 1$ denotes a pressure sensor function of the form [15]

$$\beta = 1 - \frac{|p^{(i)} - p^{(j)} + 0.5 \underline{l}^{(ji)} \cdot (\nabla p^{(i)} + \nabla p^{(j)})|}{|p^{(i)} - p^{(j)}| + |0.5 \underline{l}^{(ji)} \cdot (\nabla p^{(i)} + \nabla p^{(j)})|} \tag{37}$$

For $\beta = 0, 1$, second and fourth-order damping operators are obtained, respectively. Several forms are possible for the sensor function β [16]. Although this discretization of the adjoint Euler fluxes looks like a blend of second and fourth-order dissipation, it has no adjustable parameters.

DOI: 10.1002/fld

In the adjoint calculation, the cause-and-effect chain is traced back from the receiver (target surface Γ_{trg} carrying the cost function) to the sender (design surface Γ_{dsg} subject to shape variations). Thus, the time integral in the gradient equation (29) has to cover the period during which the shape of the design surface influences the cost function via the flowfield. Before struck by the first shock wave, the shape of the barrier wall is irrelevant to the objective, as information cannot propagate faster than the speed of the maximum eigenvalue λ. This also determines the required period of the adjoint simulation: It needs to be run in reverse time from the latest contribution to the cost function back until reaching the earliest influence of the design parameters (shape of the protective barrier Γ_{dsg}) on the flow.

7. IMPLEMENTATIONAL ISSUES

While the adjoint equations formally represent a system of advection equations with time-varying coefficients, at present it is unclear which numerical techniques are optimal when the Jacobians emanate from time-varying flow solutions with strong shocks. As stated before, the present implementation employs a simple explicit Runge–Kutta solver with second and fourth order edge-based damping. The forward integration, on the other hand, is carried out using TVD schemes with limiters. Therefore, a mismatch between the forward and adjoint solvers is possible, violating the duality principle. This implies that we do not compute the exact gradient of the discrete cost function used in the forward Euler solver due to inconsistencies in the discretization: different forward and adjoint integration schemes, interpolation between adjoint timesteps, etc. However, in the limit of infinite resolution in time and space, the inconsistencies are expected to vanish [17]. In our case this can be one reason for differences between the gradients obtained by finite- differencing and the adjoint calculus.

As we are dealing with transient problems and the complete flowfield needs to be stored in order to achieve an accurate adjoint solution, cost- and storage-effective ways of approaching this problems need to be found. To date we have simply stored the complete forward run at several hundred times, and then interpolated it when computing the adjoint. One could also contemplate the following options to ease storage requirements:

- Data compression techniques.
- Forward/backward interweaving of flow and adjoint solvers such as the so-called 'checkpointing techniques' [18, 19].
- Temporal interpolation techniques for transient problems with shocks.
- Local residual-based deactivation or removal of parts of the domain in the adjoint computation to exploit the 'narrowness' of the adjoint problem [20].

8. VERIFICATION STUDIES

The procedures described were implemented into FEFLO [21], a general-purpose, edge-based finite element code for compressible and incompressible flows. A series of verification studies was carried out. The major findings of these studies are reported in the following. Note that the time shown in the plots is the 'adjoint time', running backwards from the end of the forward simulation.

DOI: 10.1002/fld

8.1. Semi-circular object in channel

The first example considered is the quasi-2D case shown in Figure 5. The design surface to be modified is the cylinder. The main reason for this shape is that it is smooth, and thus avoids possible numerical difficulties and/or noise that may appear when sharp corners are present.

Two different initializations were considered for ambient conditions of:

$$\rho_0 = 1.0, \quad \underline{v} = (0, 0, 0), \quad e_0 = 2.5$$

(a) A 'shock-like' initialization given by:

$$\rho_1 = 2.6667, \quad \underline{v}_1 = (1.479, 0, 0), \quad e_1 = 5.3125 \quad \text{for } x \leqslant 1.2$$

(b) A 'blast-like' initialization inside the circle of radius r_0=0.15 around $\underline{x}_0$=(1.2, 0.0) given by:

$$\rho_1 = 10.0, \quad \underline{v}_1 = (0, 0, 0), \quad e_1 = 25.0$$

The cost function was the impulse (cost function $J_{\Gamma 1}$) over the target surface S0 in Figure 5(a). The element size used may be inferred from the detail of the surface mesh shown in Figure 5(b). The volume mesh had approximately 90 000 elements.

The flowfields were integrated in time (less than 5 min on a Dell desktop computer with a 3.2 GHz ITL Xeon chip, 16 GBytes of RAM, ITL compiler and Linux OS), and 100 flowfield dumps were stored. The number of 100 flowfields is, admittedly, arbitrary, but was found to be sufficient. For shock cases, which are run with explicit time-marching codes, the number of flowfields stored should be at least of the order of the number of elements connecting the source with the target. In all the cases reported here, this was the case. These 100 flowfields were used to integrate the adjoint variables backwards in time. At the same time, the gradient information was obtained and accumulated over time. Figures 5(c),(d) show the evolution of density, velocity and pressure, adjoint density, adjoint velocity and adjoint energy in time. The presence of multiple shock reflections is clearly evident.

The gradient obtained at the end of the adjoint run for the blast-like initialization is shown in Figure 5(e).

The flowfields were integrated again for cylinders with slightly smaller and larger radii ($\delta n = \pm 0.01$: as the boundary unit vector points outwards, $\delta n = 0.01$ results in a smaller radius, while $\delta n = -0.01$ increases the radius). This allowed for a comparison of the adjoint-based cost function

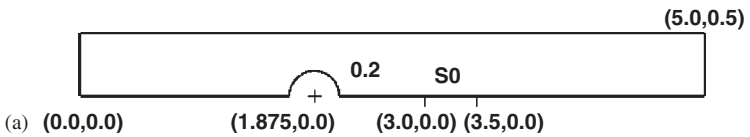

Figure 5(a): semi-circular object in channel: problem definition with dimensions (m).

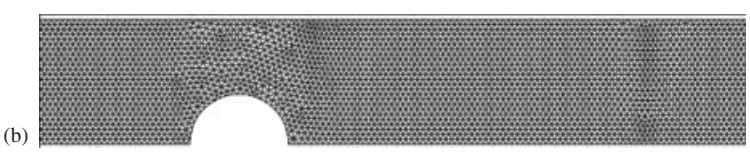

Figure 5(b): semi-circular object in channel: surface mesh.

DOI: 10.1002/fld

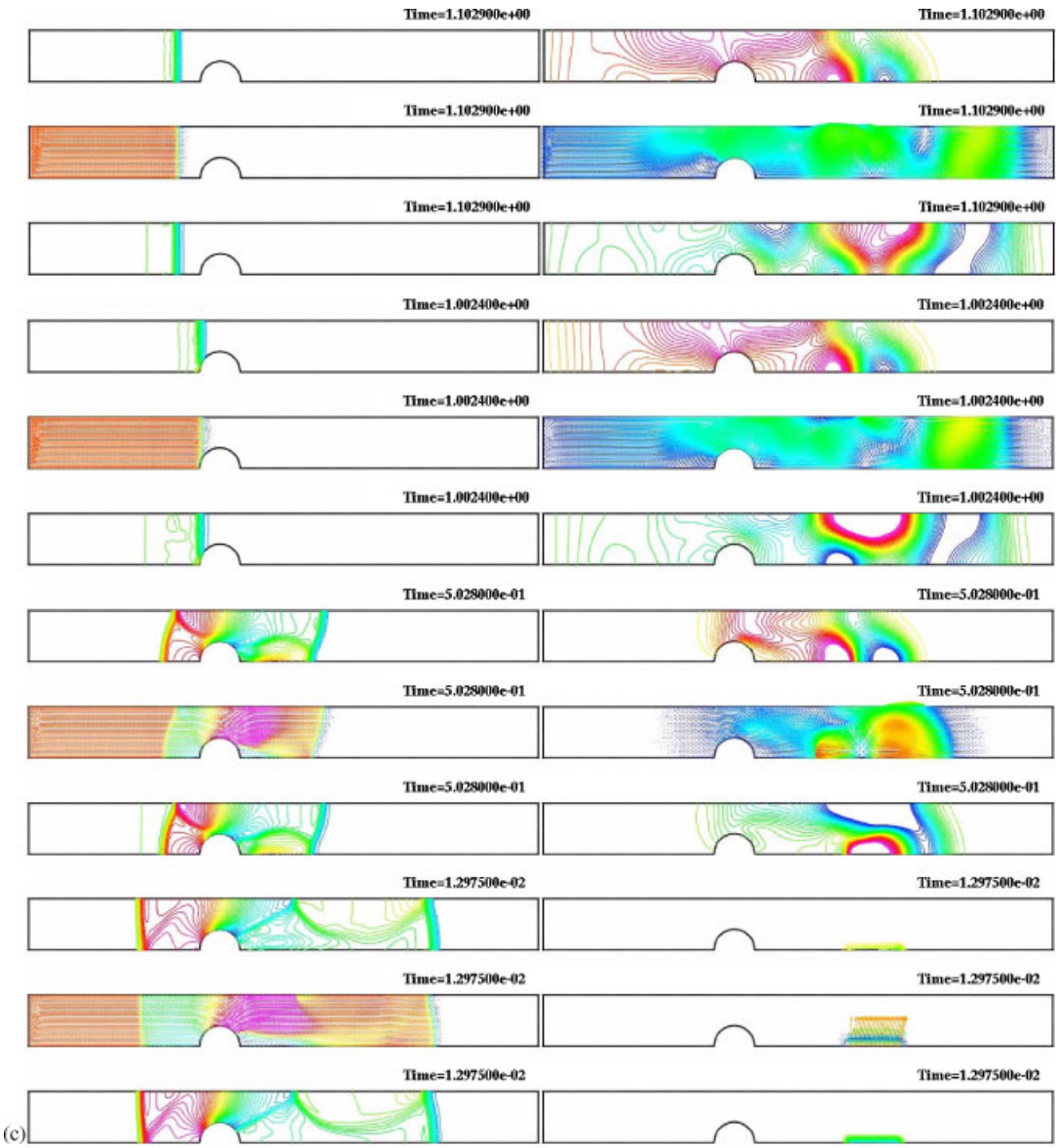

Figure 5(c): solutions at different times for shock-like initialization: left: density, velocity, pressure; right: adjoint (density, velocity, energy).

gradient with respect to the radius against a FD approximation. The comparisons are compiled in Tables I and II. Note that the first-order FDs vary considerably, while the second-order FD approximation is very close to the gradients predicted by the adjoint-based formulation. Given all other uncertainties (mesh, interpolation in time, different schemes for flow and adjoint integration, surface gradient formulation), the correlation is remarkably accurate.

DOI: 10.1002/fld

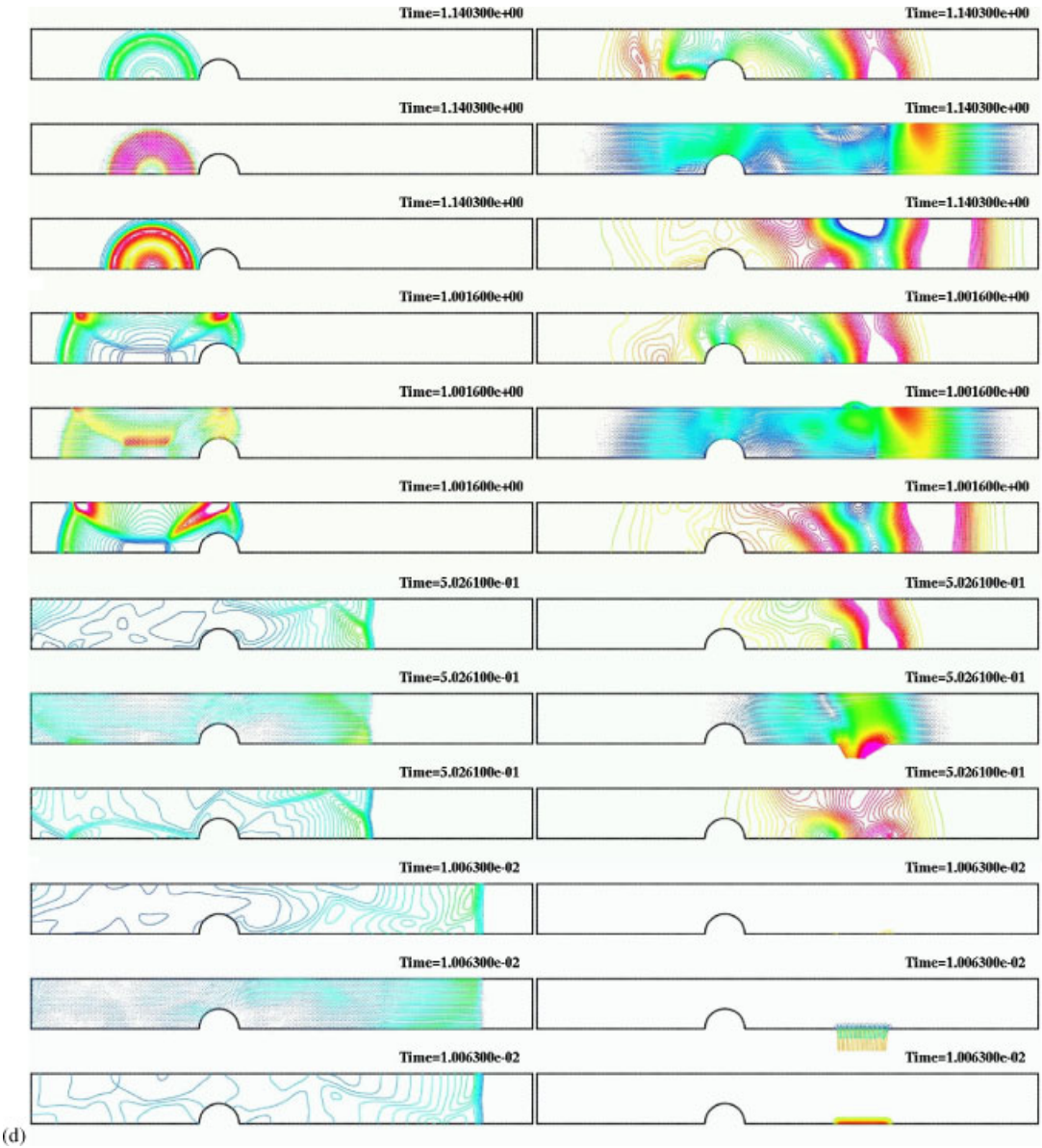

Figure 5(d): solutions at different times for blast-like initialization: left: density, velocity, pressure; right: adjoint (density, velocity, energy).

8.2. Blast wall

The geometry for this second example is shown in Figure 6(a). The units used for this and the subsequent examples are centimeters, grams and seconds (cgs). The design surface to be varied is the wall. The top of the wall is rounded in order to avoid the effects of sharp corners, and to

DOI: 10.1002/fld

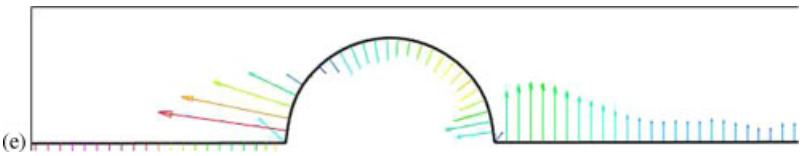

Figure 5(e): gradient $(-\delta I/\delta V)$ obtained for shock-like initialization.

Table I. Shock-like initialization: perturbation δn, cost function gradient $\delta I/\delta n$ and cost function I (impulse).

	δn or $\delta I/\delta n$	I
Impulse-larger: I_L	−0.01	−0.05811178
Impulse-normal: I_M	0.00	−0.05838425
Impulse-smaller: I_S	0.01	−0.05874545
FD: $(I_L - I_M)/\delta n$	−0.0273	
FD: $(I_S - I_M)/\delta n$	−0.0362	
FD: $0.5(I_S - I_L)/\lvert\delta n\rvert$	−0.0317	
Adjoint $\delta I/\delta n$	−0.0327	

Table II. Blast-like initialization: perturbation δn, cost function gradient $\delta I/\delta n$ and cost function I (impulse).

	δn or $\delta I/\delta n$	I
Impulse-larger: I_L	−0.01	−0.05516805
Impulse-normal: I_M	0.00	−0.05542970
Impulse-smaller: I_S	0.01	−0.05583446
FD: $(I_L - I_M)/\delta n$	−0.0261	
FD: $(I_S - I_M)/\delta n$	−0.0404	
FD: $0.5(I_S - I_L)/\lvert\delta n\rvert$	−0.0333	
Adjoint $\delta I/\delta n$	−0.0347	

allow a straightforward enlargement and shrinkage of the surface. The initialization is taken from a detailed 1-D analysis, and is interpolated to the 3-D field at the beginning of the run. The cost function was the impulse (cost function $J_{\Gamma 1}$) over surface S1 in Figure 6(a). The surface of the mesh used (approx. 1.4 million elements) is shown in Figure 6(b).

The flowfield was integrated in time (less than two hours on a Dell desktop computer with a 3.2 GHz ITL Xeon chip, 16GBytes of RAM, ITL compiler and Linux OS), and 100 flowfield dumps were stored. These were used to integrate the adjoint variables backwards in time. As before, the gradient information was obtained and accumulated over time. Figures 6(c)–(e) show the evolution of pressure and adjoint density in time.

The wall (design surface) was then enlarged and shrunk by 2.5 cm, and the flowfield was integrated again. This allowed for a comparison of the adjoint-based gradient with a FD approximation. The results obtained are summarized in Table III. Note that the first order differences

DOI: 10.1002/fld

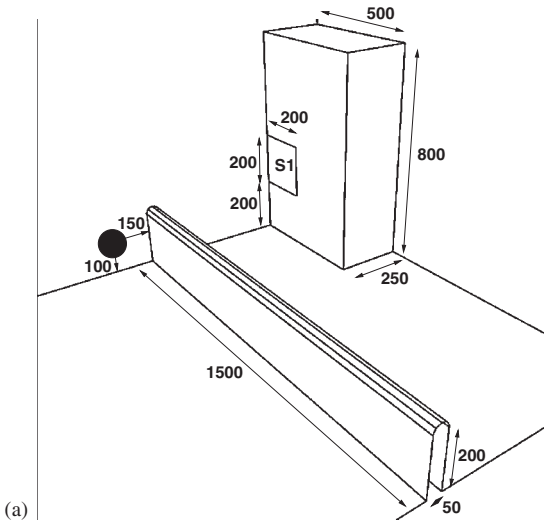

(a)

Figure 6(a): blast wall: problem definition with dimensions (cm).

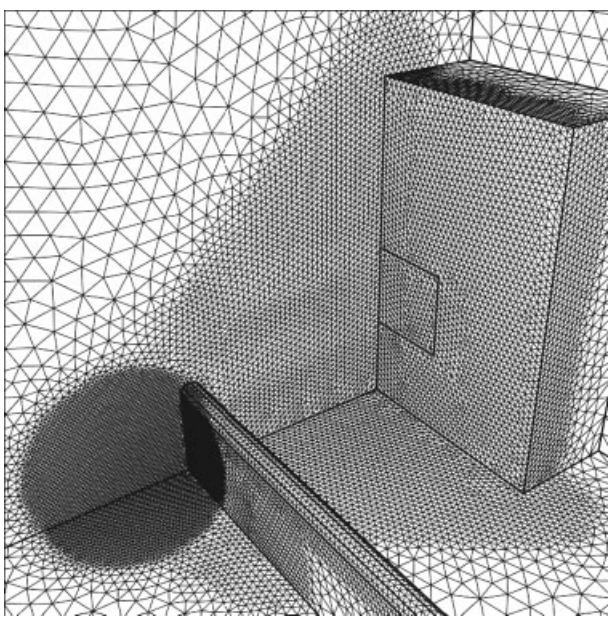

(b)

Figure 6(b): blast wall: surface mesh.

vary considerably, but that the second order FD approximation matches well the predictions of the adjoint-based formulation. The adjoint-based gradients (1) and (2), obtained from Equation (26) and the reduced gradient formulation (28), respectively, are in close agreement.

DOI: 10.1002/fld

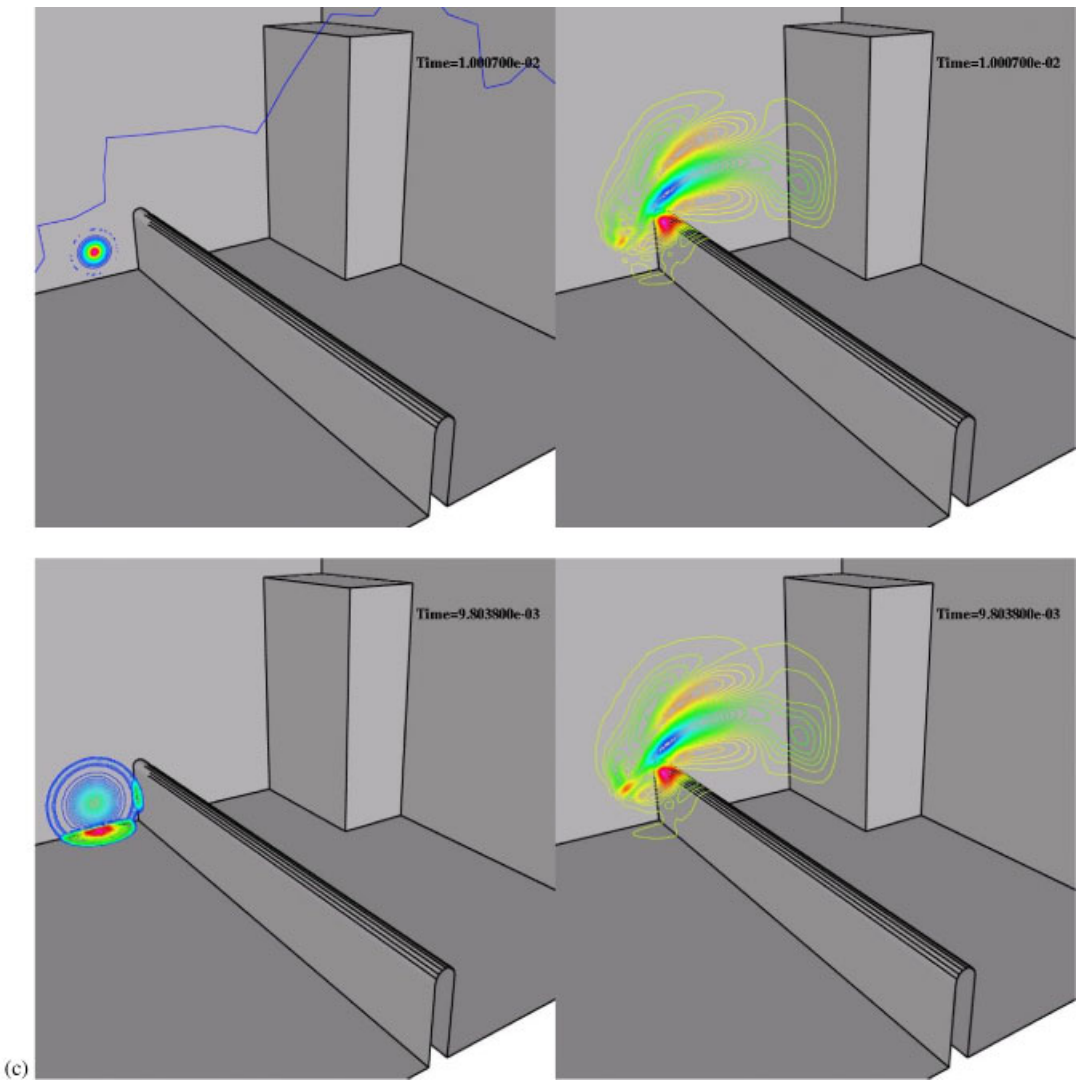

Figure 6(c): solutions at different times (left: pressure, right: adjoint density).

9. AN EXAMPLE

This case is included to demonstrate the use of the techniques proposed here to improve an existing design. It is modified manually following the negative gradient direction obtained for that particular configuration (geometry and blast definition). The improved design is probably still far from the next optimum. It could be driven toward the local optimum by using iterative optimization techniques, which is beyond the scope of this paper.

The building is the same as shown before, but now has two target windows (Γ_{trg} comprising S1 and S2, see Figure 7(a)). Subjected to the same load, it is supposed to be protected by two blast

DOI: 10.1002/fld

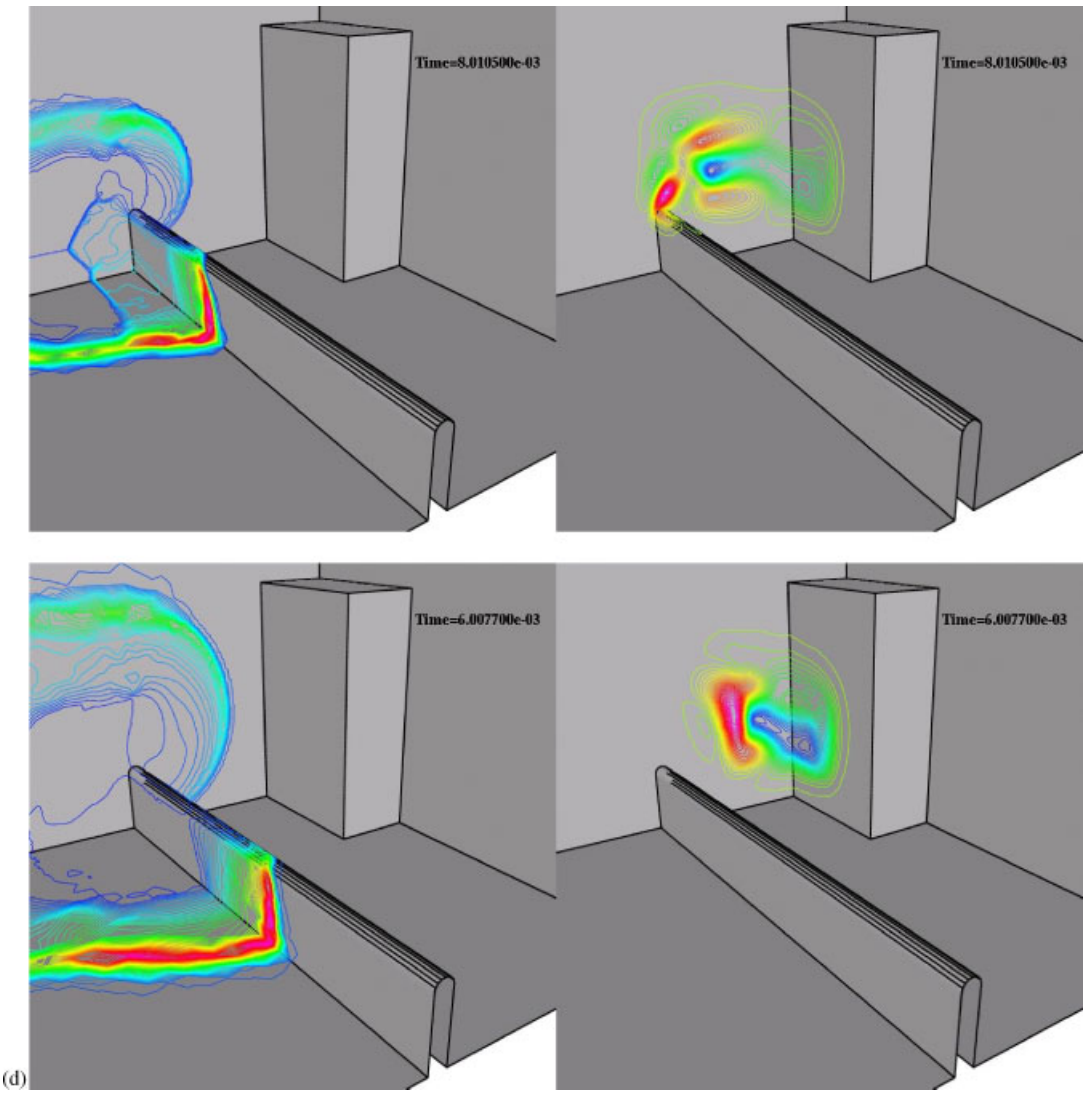

(d)

Figure 6(d): solutions at different times (left: pressure, right: adjoint density).

walls, and the question becomes: If only one of these walls is to be changed, which one should it be, and how should it be modified? Two design objectives were tested: reduction of total impulse (cost function $J_{\Gamma 1}$) and reduction in pressures above a certain threshold (cost function $J_{\Gamma 2}$).

The surface of the mesh used (approximately 1.6 million elements) is shown in Figure 7(b). The flowfield was integrated in time, and 200 flowfield dumps were stored. These were used to integrate the adjoint variables backwards in time. At the same time, the gradient information was evaluated. Figures 7(c),(d) show the evolution of pressure and adjoint density in time. The gradients

DOI: 10.1002/fld

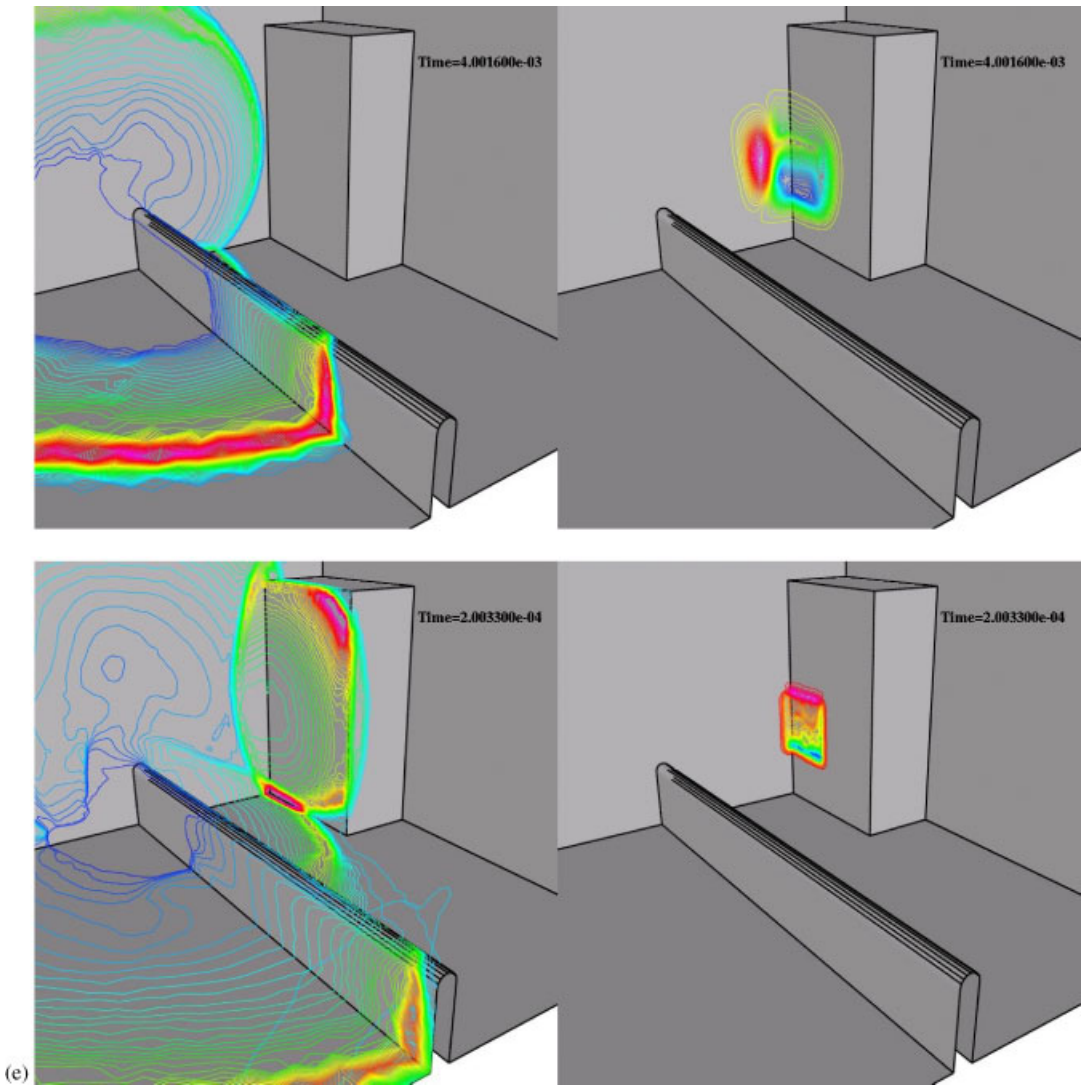

Figure 6(e): solutions at different times (left: pressure, right: adjoint density).

obtained for a pressure threshold of 1.75 times ambient pressure (cost function $J_{\Gamma 2}$) and impulse (cost function $J_{\Gamma 1}$) are compared in Figures 7(e), (f). Note that:

- The magnitudes and directions of the gradients are very similar for both cases.
- The second wall has almost no effect on the damage criteria specified; this is reflected in the very small gradients obtained.
- The first wall has a pronounced effect on the damage criteria specified; its top should be elevated and moved towards the blast origin.

DOI: 10.1002/fld

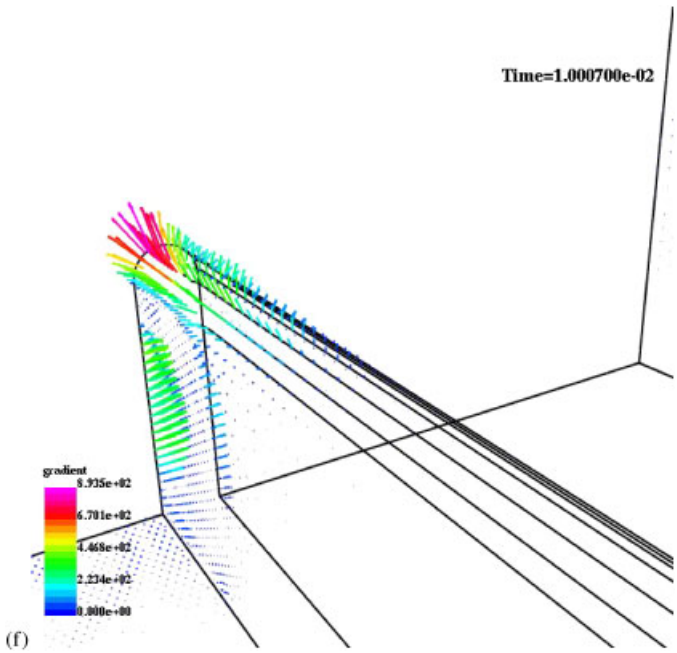

Figure 6(f): gradient of objective function: $-\delta I/\delta V$.

Table III. Blast-wall problem.

	δn or $\delta I/\delta n$	I
Impulse-larger I_L	−2.50	0.2941468E+09
Impulse-normal I_M	0.00	0.2956732E+09
Impulse-smaller I_S	2.50	0.3074946E+09
FD: $(I_L - I_M)/\delta n$	0.06105E+07	
FD: $(I_S - I_M)/\delta n$	0.47285E+07	
FD: $0.5(I_S - I_L)/\lvert\delta n\rvert$	0.26695E+07	
Adjoint (1): $\delta I/\delta n$	0.23609E+07	
Adjoint (2): $\delta I/\delta n$	0.23976E+07	

Based on these gradients, a simple change in the wall geometry was performed (see Figure 7(g)). The pressure and impulse curves obtained for the orginal and modified wall cases on the windows are compared in Figures 7(h),(i). Note the considerable effect the change has on potential damage.

10. NEW PROSPECTS AND OPPORTUNITIES

The development of the unsteady adjoint methodology opens the door to new possibilities. Some of these are discussed in the present section.

DOI: 10.1002/fld

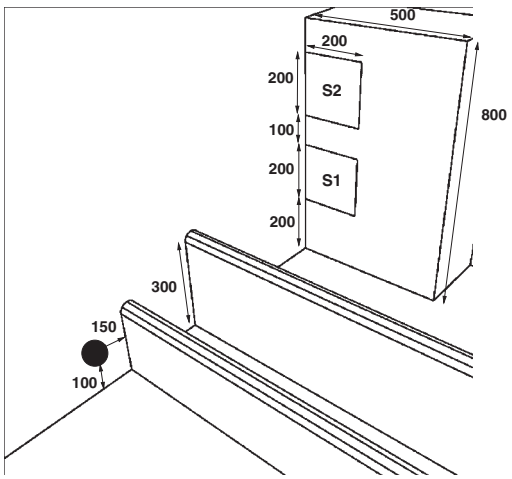

Figure 7(a): blast-walls: problem definition.

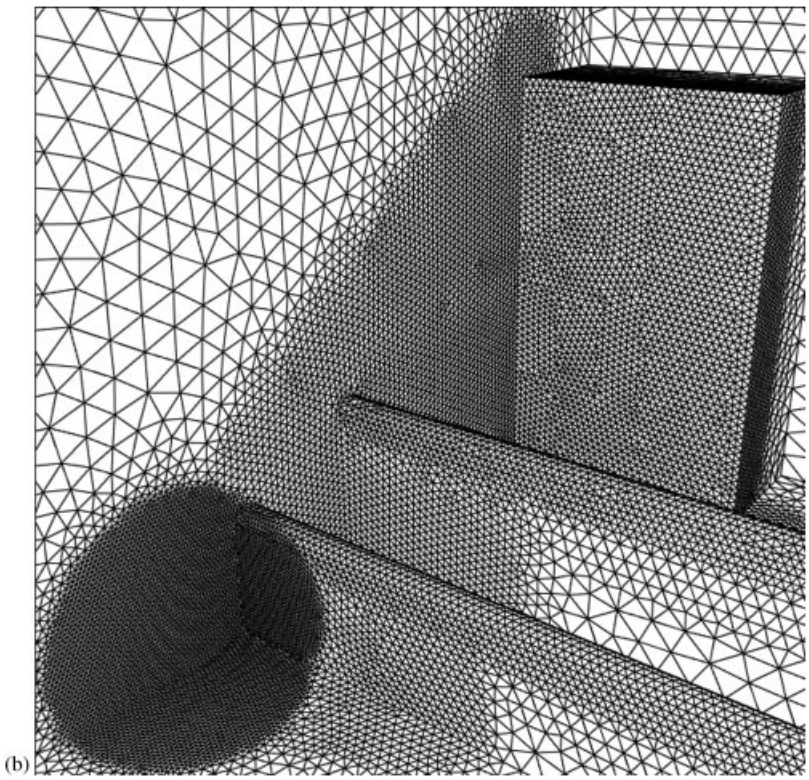

Figure 7(b): blast-walls: surface mesh.

DOI: 10.1002/fld

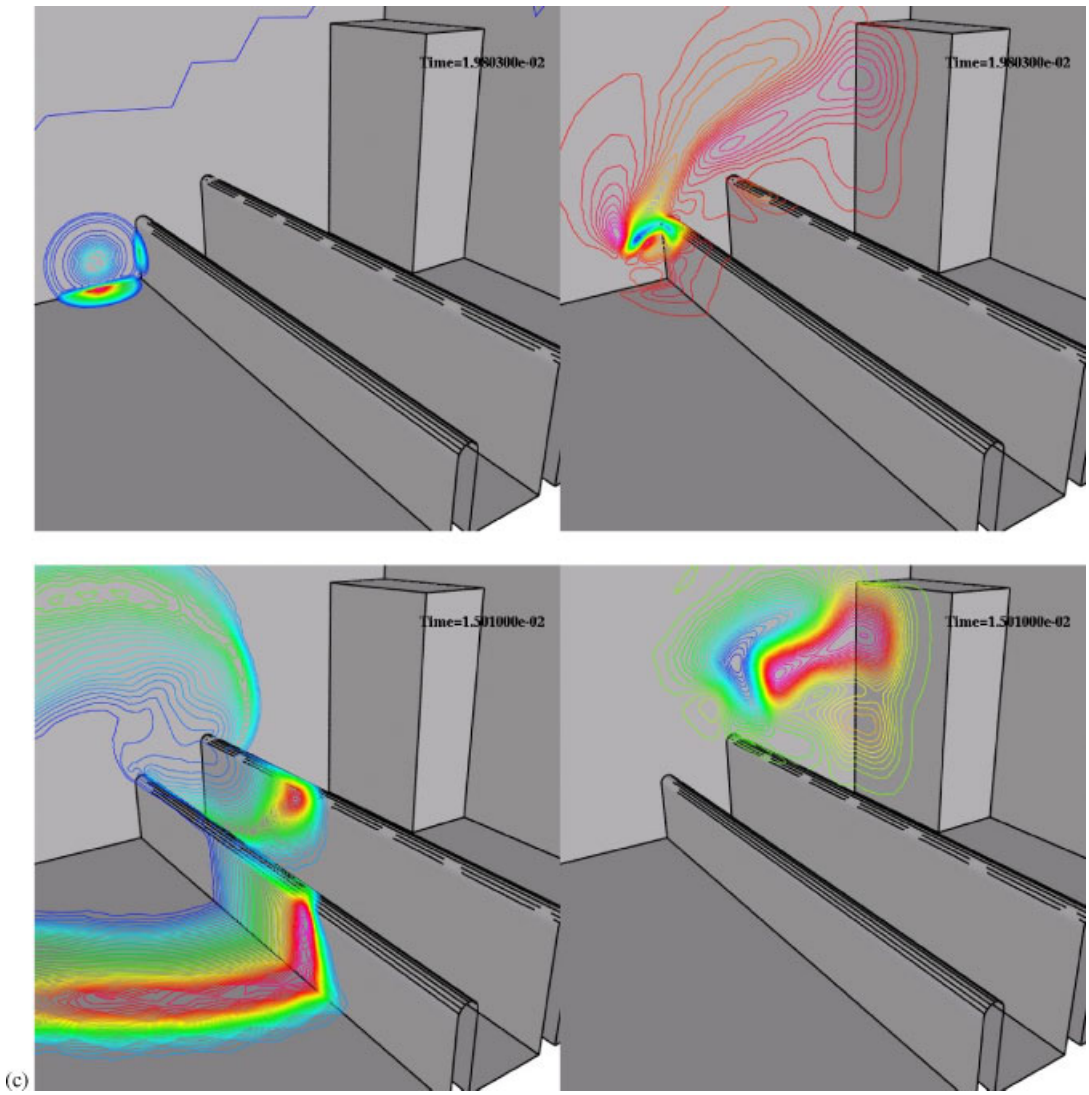

Figure 7(c): solutions at different times (left: pressure, right: adjoint density).

10.1. Instantaneous shape control

Fluid structure interaction: From Equation (29) we can derive the temporal course of the sensitivity distribution

$$\frac{\partial}{\partial t}\left(\frac{\delta J_\Gamma^{(t)}}{\delta V}\right) = -\frac{\partial v_n}{\partial n}[\rho\hat{\rho} + \rho v_i \hat{v}_i + (\rho e + p)\hat{e}] \quad \text{on } \Gamma_{\text{dsg}} \tag{38}$$

DOI: 10.1002/fld

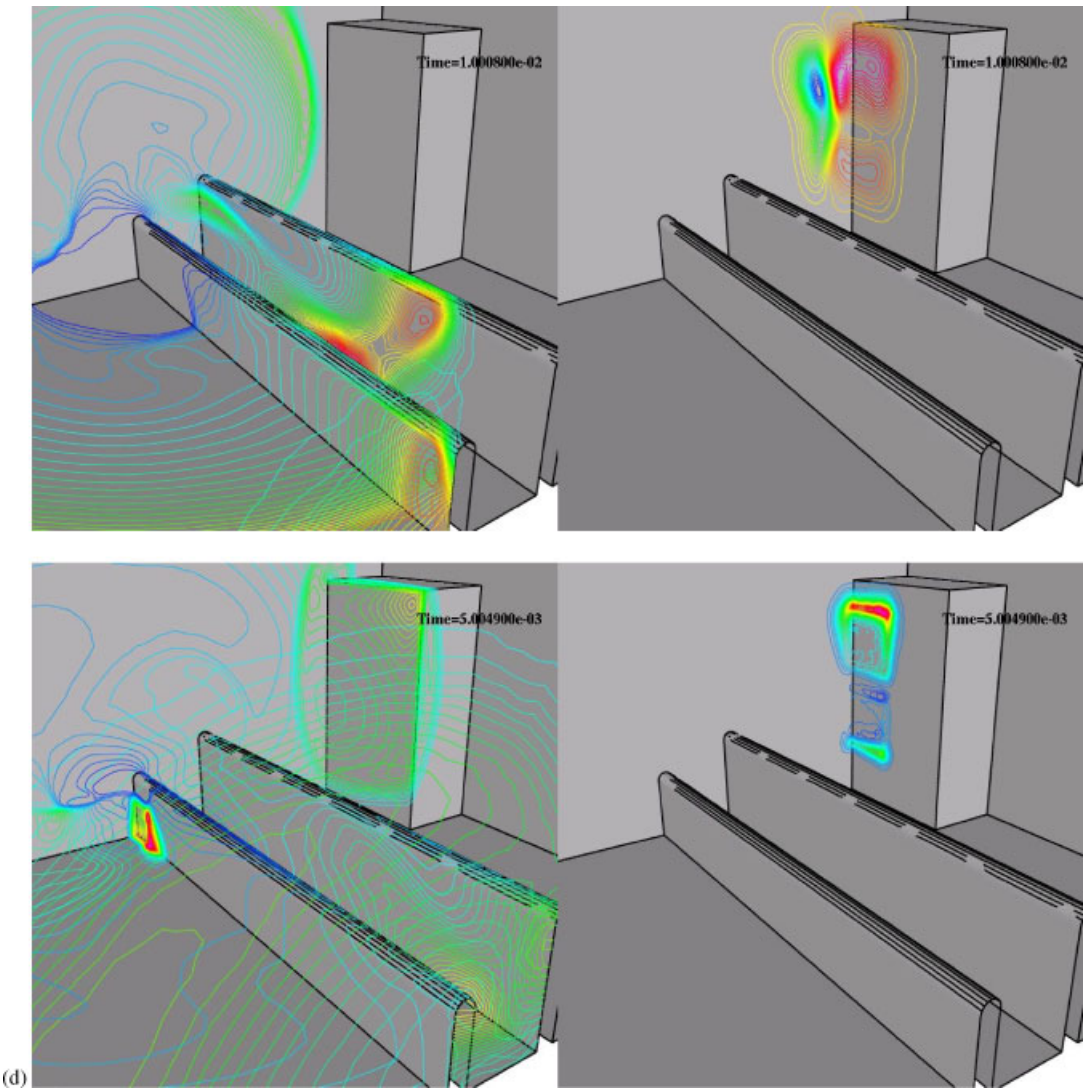

Figure 7(d): solutions at different times (left: pressure, right: adjoint density).

which can be used to find the optimal time-dependent deformation of a protective structure (passive/flexible or active/controlled). Integration over the design surface and the time interval yields the cost function variation for the applied deformation $\delta n(\underline{x}, t)$:

$$\delta J^{(t)} = \int_0^T \int_{\Gamma_{\mathrm{dsg}}} \delta n(\underline{x}, t) \frac{\partial}{\partial t} \left(\frac{\delta J_\Gamma^{(t)}}{\delta V} \right) \mathrm{d}\Gamma \, \mathrm{d}t \tag{39}$$

DOI: 10.1002/fld

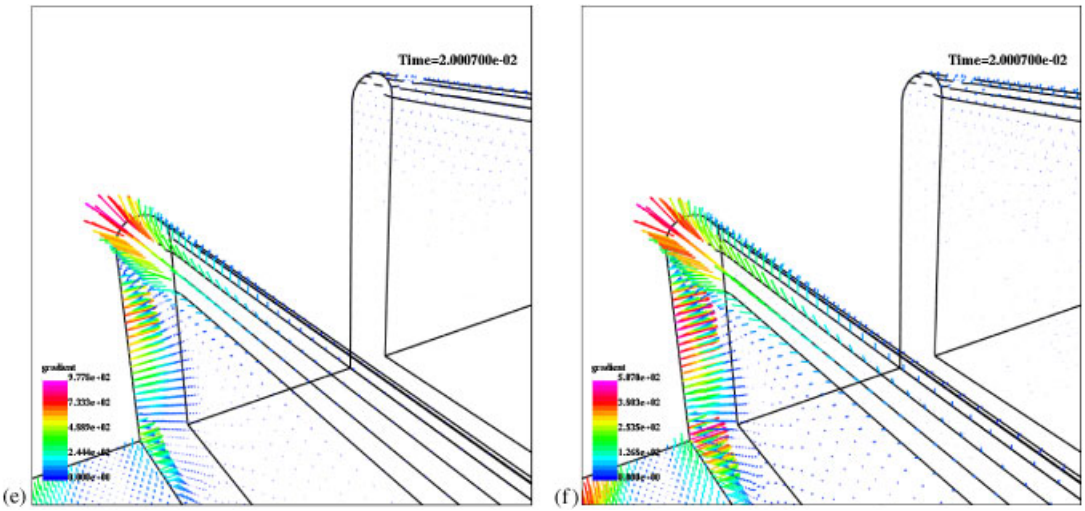

Figure 7(e,f): gradient of objective function: $-\delta I/\delta V$ (left: pressure, right: impulse).

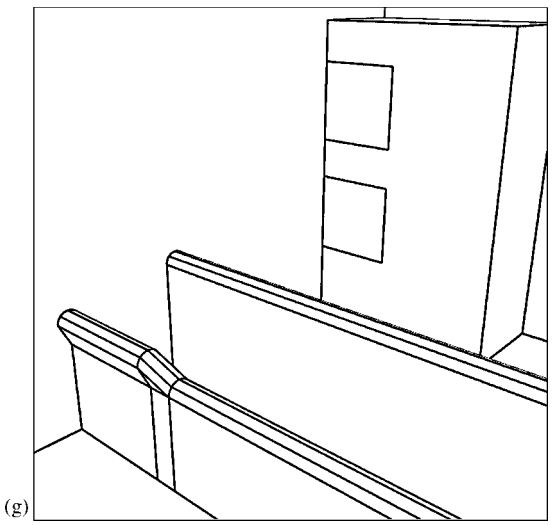

Figure 7(g): modified wall.

10.2. Variation of the explosion

Instead of controlling the blast effect on the target through the shape of the protective barrier Γ_{dsg}, it can also be controlled by local source terms $\underline{S}$ to the density, momentum or energy equation which are applied within the subvolume $\Omega_{\text{ctr}} \subset \Omega$:

$$\frac{\partial \underline{U}}{\partial t} + \frac{\partial \underline{F}_i}{\partial x_i} - \underline{S}(\underline{x}, t) = 0 \quad \text{in } \Omega_{\text{ctr}} \tag{40}$$

DOI: 10.1002/fld

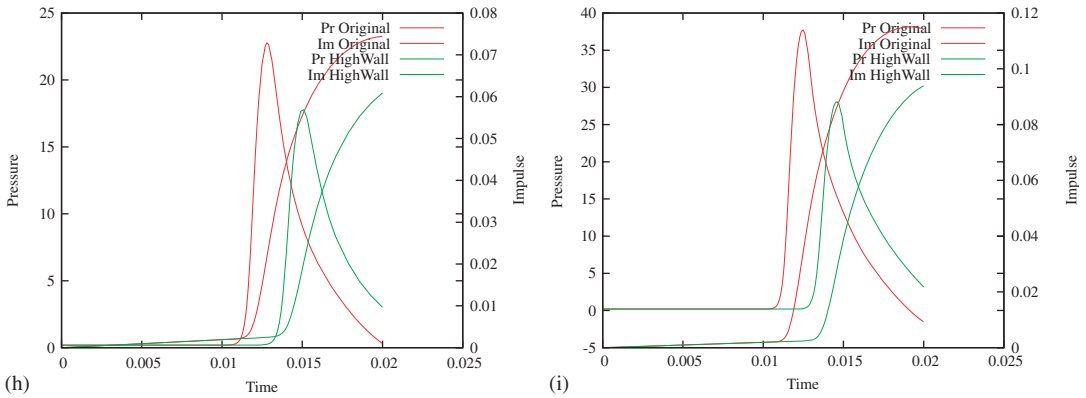

Figure 7(h,i): comparison of pressure (psi) and impulse (psi s] time histories for stations 1, 2.

In that case the domain does not undergo shape variations so that neither convective nor geometric variations exist—hence the superscripts are left out for brevity. Thus, the variation of the extended cost function reads:

$$\delta J = \int_0^T \int_{\Gamma_{\text{trg}}} \delta \underline{U} \cdot \frac{\partial j_\Gamma}{\partial \underline{U}} \, \mathrm{d}\Gamma \, \mathrm{d}t + \int_0^T \int \left[\frac{\partial \delta \underline{U}}{\partial t} + \frac{\partial}{\partial x_i} \left(\delta \underline{U} \cdot \frac{\partial \underline{F}_i}{\partial \underline{U}} \right) - \delta \underline{S}\big|_{\Omega_{\text{ctr}}} \right] \cdot \hat{\underline{U}} \, \mathrm{d}\Omega \, \mathrm{d}t \tag{41}$$

with the variation of the control $\delta \underline{S}(\underline{x}, t)$. Integration by parts yields the adjoint equations, see Equations (11a) and (12a). Note that the adjoint field equations with boundary and initial conditions remain unchanged if $\underline{S}$ is independent of $\underline{U}$. Having solved the (same!) adjoint equations, the sensitivity with respect to the source variation $\delta \underline{S}$ is obtained from

$$\delta J = -\int_0^T \int_{\Omega_{\text{ctr}}} \hat{\underline{U}} \cdot \delta \underline{S} \, \mathrm{d}\Omega \, \mathrm{d}t \tag{42}$$

The time integration (42) can be reduced to the period of active control ($\delta \underline{S} \neq 0$). Thus, the adjoint solution may be used to optimize the following applications:

- When the explosion is induced through source terms $\underline{S}$ in the Euler equations after the initialization, a spatial variation of the explosion by $\delta \underline{x}$ can be expressed through a source variation $\delta \underline{S}$. This leads to the modified sources:

$$\underline{S}'(\underline{x}) = \underline{S}(\underline{x} - \delta \underline{x}) = \underline{S}(\underline{x}) + \delta \underline{S}(\underline{x}) = \underline{S}(\underline{x}) + \delta \underline{x} \cdot \frac{\delta \underline{S}}{\delta \underline{x}} \quad \text{in } \Omega_{\text{ctr}} \tag{43}$$

  The matrix $\delta \underline{S} / \delta \underline{x}$ links a spatial variation of the source $\delta \underline{S}$ to the corresponding offset $\delta \underline{x}$. Thus, the cost function sensitivity with respect to a displacement of the explosion is obtained from

$$\delta J = \delta \underline{x} \cdot \frac{\delta J}{\delta \underline{x}} = -\int_0^T \int_{\Omega_{\text{ctr}}} \delta \underline{x} \cdot \frac{\delta \underline{S}}{\delta \underline{x}} \cdot \hat{\underline{U}} \, \mathrm{d}\Omega \, \mathrm{d}t \tag{44}$$

DOI: 10.1002/fld

- The adjoint solution $\underline{\hat{U}}$ represents the sensitivity of the objective function with respect to the residual $\delta\underline{S}(\underline{x}, t)$ in time and space, compare Equation (42). Therefore, looking at the adjoint field solution tells the designer when and where to introduce sources $\delta\underline{S}$ of mass, momentum or energy to control the effect on the target. These could for example be given by secondary explosions.

11. CONCLUSIONS AND OUTLOOK

Unsteady Euler and adjoint Euler solvers have been combined in order to aid in the design of shock mitigation devices. The results obtained to date indicate that this is a very cost-effective way to obtain the gradients of an objective function with respect to surface design changes. As the information is evaluated over a complete surface, the procedure provides considerable insight, and can thus aid in the design of architecturally appealing blast walls.

On the other hand, a number of improvements will be required in order to transfer these techniques into a production environment. Among these, we mention:

- Improved adjoint solvers for the unsteady Euler equations with strong shocks (time integration, limiting, Riemann solvers, etc.) [7].
- Optimal storage techniques for the unsteady 3-D flowfield (data compression, interpolation with limiting in time, etc.).
- Interweaved forward–backward integration of the flow and adjoint equations [18, 19].

APPENDIX A

A.1. Adjoint boundary conditions

The cost-function-specific adjoint boundary conditions are obtained by eliminating the boundary contributions to Equation (12) with $v_i n_i = \delta v_i^{(l)} n_i = 0$ on $\Gamma \backslash \Gamma_{\mathrm{dsg}}$. Expansion of the integrand in (12b) yields

$$0 = (\delta\rho^{(l)}\hat{\rho}v_i + \rho\hat{\rho}\delta v_i^{(l)} + \delta\rho^{(l)}\hat{v}_j v_j v_i + \rho\hat{v}_j \delta v_j^{(l)} v_i + \rho\hat{v}_j v_j \delta v_i^{(l)} + \delta\rho^{(l)}\hat{v}_i$$
$$+ [\rho e + p]\hat{e}\delta v_i^{(l)} + \hat{e}v_i[\rho\delta e^{(l)} + e\delta\rho^{(l)} + \delta p^{(l)}])n_i + \underline{\delta p^{(l)} \frac{\partial j_\Gamma}{\partial p}} \quad \text{on } \Gamma \backslash \Gamma_{\mathrm{dsg}} \tag{A1}$$

The underlined term above is only declared on Γ_{trg} and does not contribute elsewhere. Thus, the adjoint boundary condition for all wall faces not contributing to the cost function (and this may be time-dependent) is

$$\hat{v}_i n_i = 0 \quad \text{on } \Gamma \backslash \Gamma_{\mathrm{trg}} \tag{A2}$$

and for all wall faces contributing to the cost function (again, this may be time-dependent):

$$\hat{v}_i n_i = -\frac{\partial j_\Gamma}{\partial p} \quad \text{on } \Gamma_{\mathrm{trg}} \tag{A3}$$

DOI: 10.1002/fld

That is, depending on the cost function definition, the adjoint boundary conditions may change during the simulation time. The remaining adjoint boundary conditions (outlet/far-field) are the same as in the steady case and can be taken from [13].

On Γ_{dsg} the cost function gradient is evaluated from the boundary terms (12b) using the same adjoint boundary conditions together with $\delta v_n^{(l)} = -\delta n(\partial v_n/\partial n)$ as shown in A.2.

A.2. Reduced gradient equation

Expansion of Equation (26) yields

$$\begin{aligned}\delta J^{(t)} &= \int_0^T \int_{\Gamma_{\mathrm{dsg}}} \delta \underline{U}^{(l)} \cdot \frac{\partial \underline{F}_i}{\partial \underline{U}} \cdot \underline{\hat{U}} n_i \,\mathrm{d}\Gamma \,\mathrm{d}t \\ &= \int_0^T \int_{\Gamma_{\mathrm{dsg}}} (\delta\rho^{(l)}\hat{\rho} v_i + \rho\hat{\rho}\delta v_i^{(l)} + \delta\rho^{(l)}\hat{v}_j v_j v_i + \rho\hat{v}_j \delta v_j^{(l)} v_i + \rho\hat{v}_j v_j \delta v_i^{(l)} + \delta p^{(l)}\hat{v}_i \\ &\quad + [\rho e + p]\hat{e}\delta v_i^{(l)} + \hat{e} v_i [\rho \delta e^{(l)} + e\delta\rho^{(l)} + \delta p^{(l)}]) n_i \,\mathrm{d}\Gamma \,\mathrm{d}t \end{aligned} \tag{A4}$$

With (27) and $v_n = \hat{v}_n = 0$ over Γ_{dsg}, it reduces to

$$\frac{\delta J^{(t)}}{\delta n} = \int_0^T \int_{\Gamma_{\mathrm{dsg}}} -\frac{\partial v_n}{\partial n} [\rho\hat{\rho} + \rho v_i \hat{v}_i + (\rho e + p)\hat{e}] \,\mathrm{d}\Gamma \,\mathrm{d}t \tag{A5}$$

Together with

$$\frac{\partial \underline{F}_n}{\partial n} = \begin{pmatrix} v_n \dfrac{\partial \rho}{\partial n} + \dfrac{\partial v_n}{\partial n}\rho \\ v_n \dfrac{\partial \rho v_i}{\partial n} + \rho v_i \dfrac{\partial v_n}{\partial n} + \dfrac{\partial p}{\partial n} n_i \\ (\rho e + p) - \dfrac{\partial v_n}{\partial n} + \left(\dfrac{\partial \rho e}{\partial n} + \dfrac{\partial p}{\partial n}\right) v_n \end{pmatrix} = \begin{pmatrix} \rho \\ \rho v_i \\ \rho e + p \end{pmatrix} \frac{\partial v_n}{\partial n} + \begin{pmatrix} 0 \\ \dfrac{\partial p}{\partial n} n_i \\ 0 \end{pmatrix} \quad \text{on } \Gamma_{\mathrm{dsg}} \tag{A6}$$

expression (A5) is equivalent to:

$$\frac{\delta J^{(t)}}{\delta n} = \int_0^T \int_{\Gamma_{\mathrm{dsg}}} -\frac{\partial \underline{F}_n}{\partial n} \cdot \underline{\hat{U}} \,\mathrm{d}\Gamma \,\mathrm{d}t \tag{A7}$$

A.3. Evaluation of gradient II

When the adjoint equations are satisfied, an alternative form of the gradient equation is

$$\frac{\delta J^{(t)}}{\delta n} = \int \int \underline{R}_{,n} \cdot \underline{\hat{U}} \,\mathrm{d}\Omega \,\mathrm{d}t \tag{A8}$$

DOI: 10.1002/fld

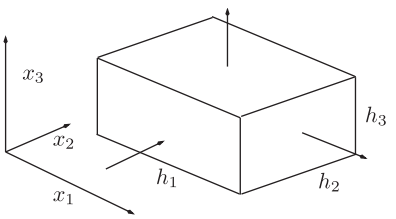

Figure A1. Finite volume approximation close to wall.

Several formulations have been proposed [12, 13]. Based on the discretization shown in Figure A1, a simple control volume discretization may be written as:

$$\begin{aligned}\underline{R}\Delta\Omega &= h_1h_2h_3\,\underline{U}_{,t} + \sum_{\text{faces } j} (\Delta\Gamma\, n_i\, \underline{F}_i)_j \\ &= h_1h_2h_3\,\underline{U}_{,t} + h_2h_3[\underline{F}_1(x_1+h_1) - \underline{F}_1(x_1)] \\ &\quad + h_1h_3[\underline{F}_2(x_2+h_2) - \underline{F}_2(x_2)] + h_1h_2[\underline{F}_3(x_3+h_3) - \underline{F}_3(x_3)] \\ &= 0 \end{aligned} \tag{A9}$$

If we move the upper surface by a small normal offset δn_3 in the x_3 direction without altering the fluxes, the residual becomes:

$$\begin{aligned}\underline{R}'\,\Delta\Omega &= (h_3+\delta n_3)h_1h_2\,\underline{U}_{,t} + (h_3+\delta n_3)h_2\,[\underline{F}_1(x_1+h_1) - \underline{F}_1(x_1)] \\ &\quad + (h_3+\delta n_3)h_1\,[\underline{F}_2(x_2+h_2) - \underline{F}_2(x_2)] + h_1h_2\,[\underline{F}_3(x_3+h_3) - \underline{F}_3(x_3)] \end{aligned} \tag{A10}$$

Therefore, the leading term in the normal derivative is:

$$\begin{aligned}\underline{R}_{,n}\Delta\Omega = \frac{\underline{R}' - \underline{R}}{\delta n_3}\Delta\Omega &= h_1h_2\,\underline{U}_{,t} + h_2\,[\underline{F}_1(x_1+h_1) - \underline{F}_1(x_1)] + h_1\,[\underline{F}_2(x_2+h_2) - \underline{F}_2(x_2)] \\ &= h_1h_2\,[\underline{U}_{,t} + \underline{F}_{1,1} + \underline{F}_{2,2}] \end{aligned} \tag{A11}$$

and, by virtue of the original conservation law (4):

$$\underline{R}_{,n}\Delta\Omega = -h_1h_2\,\underline{F}_{3,3} = -h_1h_2\,\underline{F}_{n,n} = -\underline{F}_{n,n}\,\Delta\Gamma \tag{A12}$$

This expression is then used in Equation (A8) to obtain the cost function sensitivity $\delta J^{(t)}/\delta n$. It is obvious that this control volume-based derivation leads to the same approximations for the gradient equations as devised in Section 4, compare expression (A7) with (A12) applied to (A8).

REFERENCES

1. Jameson A. Optimum aerodynamic design using CFD and control theory. *AIAA-95-1729-CP*, 1995.
2. Reuther J, Jameson A, Farmer J, Matinelli L, Saunders D. Aerodynamic shape optimization of complex aircraft configurations via an adjoint formulation. *AIAA-96-0094*, 1996.
3. Newman JC, Taylor AC, Barnwell RW, Newman PA, Hou GJ. Overview of sensitivity analysis and shape optimization for complex aerodynamic configurations. *Journal of Aircraft* 1999; **36**(1):87–96.

DOI: 10.1002/fld

4. Nielsen E, Anderson W. Recent improvements in aerodynamic design and optimization on instructured meshes. *AIAA-01-0596*, 2001.
5. Mohammadi B, Pironneau O. *Applied Shape Optimization for Fluids*. Oxford University Press: Oxford, 2001.
6. Soto O, Löhner R, Yang C. An adjoint-based design methodology for CFD problems. *International Journal for Numerical Methods in Fluids* 2004; **14**(6):734–759.
7. Löhner R. *Applied CFD Techniques* (2nd edn). Wiley: New York, 2008.
8. Goldberg DE. *Genetic Algorithms in Search*, *Optimization and Machine Learning*. Addison-Wesley: Reading, MA, 1989.
9. Deb K. *Multi-objective Optimization Using Evolutionary Algorithms*. Wiley: New York, 2001.
10. De Jong K. *Evolutionary Computing*. MIT Press: Cambridge, MA, 2006.
11. Tsuga T, Löhner R, Togashi F. Multi-objective assessment of blast damage. *Proceedings of the MABS-20 Conference*, Oslo, Norway, September 2008.
12. Jameson A, Kim S. Reduction of the adjoint gradient formula in the continuous limit. *AIAA-03-0040*, 2003.
13. Soto O, Löhner R. On the computation of flow sensitivities from boundary integrals. *AIAA-04-0112*, 2004.
14. Roe PL. Approximate riemann solvers, parameter vectors and difference schemes. *Journal of Computational Physics* 1981; **43**:357–372.
15. Peraire J, Peiro J, Morgan K. A three-dimensional finite element multigrid solver for the Euler equations. *AIAA-92-0449*, 1992.
16. Mestreau E, Löhner R, Aita S. TGV tunnel-entry simulations using a finite element code with automatic remeshing. *AIAA-93-0890*, 1993.
17. Nadarajah S, Jameson A. Studies of the continuous and discrete adjoint approaches to viscous automatic aerodynamic shape optimization. *AIAA-2001-2530*, 2001.
18. Giering R, Kaminski T. Recipes for adjoint code construction. *ACM Transactions of Mathematical Software* 1998; **24**(4):437–474.
19. Sternberg J. Reduction of storage requirement by checkpointing for time-dependent optimal control problems. *Ph.D. Thesis*, Technische Universität Dresden, 2005.
20. Löhner R, Luo H, Baum JD, Rice D. Improvements in speed for explicit, transient compressible flow solvers. *International Journal for Numerical Methods in Fluids* 2008; **56**(12):2229–2244.
21. Löhner R, Yang C, Cebral J, Soto O, Camelli F, Baum JD, Luo H, Mestreau E, Sharov D. Advances in FEFLO. *AIAA-02-1024*, 2002.

DOI: 10.1002/fld